Detection of metal-molecule-metal junction formation by surface enhanced Raman spectroscopy

Nungnit Wattanavichean, Matthew Gilby, Richard J. Nichols, Heike Arnolds*.

Department of Chemistry, University of Liverpool, Crown Street, Liverpool L69 7ZD, UK

ABSTRACT: Vibrational modes play a key role in characterizing metal-molecule-metal junctions, but their detection currently either requires single-molecule sensitivity or the generation of defect-free large-scale junctions. Here we demonstrate that surface-enhanced Raman scattering (SERS) on non-ideal surfaces can provide a significant amount of information despite many defects in the layer. We determine the vibrational signature of the molecular electronic junction for palladium ions complexed and reduced on 4-mercaptopyridine adsorbed on rough gold and gold nanoparticles using SERS and density functional theory (DFT). We show that these non-ideal surfaces can be used to probe kinetics of metal ion complexation and establish the success of electrochemical metallization. SERS on non-ideal surfaces is thus revealed as a useful tool to rapidly establish the key process parameters in making molecular electronic junctions before embarking on more detailed studies on single molecules or single crystal surfaces.

Keywords: Metal-molecule-metal junctions, surface-enhanced Raman spectroscopy, 4-mercaptopyridine, gold

Metal-molecule-metal junctions are of great current interest as it is hoped that molecules can surpass silicon for functionality[1,2]. These junctions have been characterized by many techniques, mainly focusing on electronic states and conductance properties[3,4].

While electronic states are of primary importance for molecular conductance, detection of vibrational modes is becoming more important for full understanding of the junction behavior. At a basic level, vibrational spectroscopy of metal-molecule-metal junctions shows whether the molecule remains intact and whether any new vibrational modes in the spectrum indicate actual bond formation between a functional group and a metal layer. Moreover, in the context of molecular electronics, it permits detecting the effect of an applied electric field on the molecular structure or any coupling between electronic transport in the junction and vibrational modes[5,6].

Several different experimental approaches are in current use. In inelastic tunneling spectroscopy (IETS) electrons tunneling between a substrate and a tip can lose energy by exciting a molecular vibration, thus tunneling into a different empty electronic state. This inelastic tunneling channel increases the conductance and becomes visible as a peak in the d^2I/dV^2 curve as a function of bias potential. IET spectra were found to agree well with Raman spectra[7], and it could be shown that only longitudinal vibrational modes couple to the tunneling electrons. Total internal reflection IR spectroscopy can be used if one of the contacting electrodes is a semiconductor transparent to infrared light, such as silicon [8-10], for example to understand the molecular origin of rectification in nitroazobenzene junctions[11]. Sum frequency spectroscopy has been applied to similar systems and has the advantage compared to FTIR that it can reveal the change in molecular order as the metal overlayer is deposited. For example, gold vapor deposition on an alkane SAM introduces a large number of gauche defects, explained by metal creep in these layers[12]. A more common approach to study metal-molecule-metal junctions is gap-mode Raman spectroscopy, which uses the strong electric-field enhancement in a metallic nanogap to detect Raman spectra of few or even single molecules[13-19]. Nanogaps can be created by nanofabrication, deposition of gold nanoparticles or a metallic tip (tip-enhanced Raman spectroscopy, TERS). Molecules have even been deposited at the internal junction of a core-shell nanoparticle[20].

Many of these studies have investigated the relationship between junction bias and vibrational spectrum, but surprisingly few have focused on the fundamental issue of detecting a vibrational signature for the contact formed between the molecule and the top electrode. Junction formation between bipyridine and mercaptopyridine SAMs on gold and gold nanoparticles has been deduced from spectral changes in SERS[21,22]. However, a decided disadvantage of such gap-mode Raman is the occurrence of plasmon-induced photochemical reactions of molecules in the hot spots between nanoparticles[23]. The intermediate step to metallization, complexation of metal ions to mercaptopyridine SAMs has revealed new vibrational modes[24,25].

The lack of work in this area is partly due to the experimental challenges of either preparing large area defect-free metal-molecule-metal layers, which can be analyzed with infrared or sum frequency generation, or alternatively detecting a single molecule in TERS or IETS.

We show here that there is a third option – analyzing a collection of small-scale junctions on non-ideal roughened or nanoparticle surfaces suitable for surface-enhanced Raman scattering (SERS). We specifically look at the example of 4-mercaptopyridine (pySH) sandwiched between gold and a transition metal layer, electrochemically deposited via the Kolb method highlighted below.

Early efforts to create large-scale junctions used metal vapor deposition[26-28], however, in most cases permeation of metal through the self-assembled monolayer (SAM) could not be prevented. Electrochemical deposition offers more control of the process although metal creeping underneath the SAM is still an often-encountered problem[29-33]. A highly successful variation of the electrochemical deposition approach was developed by the Kolb group[34-36]. The technique is a two-step deposition, where metal ions coordinate to a pyS SAM in metal salt solution (Pt, Rh, Pd) before sample transfer to a dilute metal-free electrolyte for electrochemical reduction. The metal ions serve as nucleation centers for growth of metal clusters, which prevents metal diffusion into the SAM[37] and leads to smaller metal clusters compared to the one-step

method[38]. The formation of relatively stable solvent complexes, e.g $Pd(H_2O)_2$, also serves to stop vertical diffusion through the layer and facilitates horizontal diffusion[39]. Variations of the technique involve electrochemical reduction in low metal salt concentration[40] or the use of molecular hydrogen for a gentler reduction[41]. The concept was extended to more complicated structures such as a Pt-pyS-Pd-pyS-Au doubledecker[42] and different linkers such as thiazole[43] or pyridine-terminated araliphatic thiols[40,44].

Here we use the Kolb method to prepare transition metal – pyS – gold junctions on SERS-active roughened gold and also investigate metal ions complexed to 4-mercaptopyridine adsorbed at gold nanoparticles. The non-ideality of the roughened or nanoparticle surfaces manifests itself in spectra which are the sum of metallized and bare SAMs. With the help of DFT we manage to identify the origins of each peak clearly. The identification of new vibrational modes caused by complexation of metal ions allow us to follow complexation kinetics, estimate the fraction of layer that is metallized, and monitor electrochemical reduction. While rough surfaces show a slightly different electrochemical behavior to single crystal surfaces due to defects in the SAM, the surface-enhanced Raman spectra themselves show little influence from metal creep.

EXPERIMENTAL SECTION

Substrate preparation

All glassware was soaked in 70 °C Piranha solution (30 % H_2O_2 + 70 % H_2SO_4) for an hour to eliminate all organic residues. After cleaning, the glassware was rinsed with ultrapure water (18.2 MΩ, Merck Millipore, UK) and dried with nitrogen gas. Polycrystalline gold foil (99.95% purity) (Advent Research Materials) was electrochemically roughened in 0.1 M KCl. Shell isolated nanoparticles (SHINs) were prepared according to the standard Nature protocol[45] with a relatively thin shell which contains pinholes for pySH adsorption, but at the same time stops nanoparticle aggregation through bridging molecules. SHINs were deposited and dried on a Piranha-cleaned silicon wafer. PyS was removed from gold wires by running the sample as a working electrode with a gold counter electrode and Ag/AgCl reference electrode in 0.1 M NaOH[46].

Adsorption and complexation

To create the self-assembled monolayer we used 4,4'-dipyridyl disulfide (Aldrithiol-4 (98% purity)) as supplied by Sigma-Aldrich (Poole, UK), in a 40 μM solution prepared in hot, ultrapure water. Gold wire or dried SHINs on a silicon wafer were typically immersed in pyS solution for 5 minutes at room temperature. The disulfide bond has been shown to break on adsorption and form a thiolate[47]. The sample was then removed from solution, rinsed with ultrapure water and transferred to 1 mM metal salt solution. $PdSO_4$ and K_2PtCl_4 were prepared in 0.1 M H_2SO_4, while $RhCl_3$ was prepared in 0.1 M HCl [35,48,49]for typically 30 minutes. After complexation, substrates were rinsed and then transferred to an electrochemical cell at + 0.7 V vs SCE and reduced by scanning to – 0.2 V vs SCE in 0.1 M H_2SO_4 or metal salt solution to reduce the metal ion complex to solid metal.

SERS characterization

Raman spectra were mainly acquired with a Mini Ram II (B&W Tek) with 785 nm laser. Fig. 4 and Fig. 6A data were acquired with a Renishaw in-Via microscope with 785 nm laser.

To account for any changes in sample position during the measurement, we normalize the SER spectra by the background value at 915 cm^{-1} (peak-free region) and subtract a polynomial background before calculating the difference spectrum[50]. Alternatively, surface-enhanced elastic scattering can be used for spectra normalization.[51]

Calculations

Raman spectra were calculated using density functional theory (DFT) with Spartan 16 software, using the B3LYP hybrid functional with 6-31G** basis set. We have previously used this to describe hydrogen bonding in mercaptopyridine SAMs on gold[50] and found that the frequencies calculated by Birke and Lombardi for pyS on silver are also reproduced very well[52]. The only exception is the frequency of the metal substrate-molecule stretch because the surface is modelled as a single atom.

Safety considerations

Piranha solution: adding sulfuric acid to hydrogen peroxide is a strongly exothermic process and containers quickly become too hot to touch. The solution is highly corrosive and can form explosive mixtures with organic compounds and only the smallest amount needed for cleaning should be prepared. Piranha solution should not be stored in closed containers due to gas evolution. Raman laser: we used output powers between 20 and 150 mW. 1 mW is the safe limit for direct viewing of a low divergence visible laser beam for 0.25 s (blink reflex). Since 785 nm is at the edge of the visible range, stray reflections from roughened surfaces could exceed the maximum permissible exposure and the sample should not be directly viewed without laser safety goggles.

RESULTS AND DISCUSSION

Spectral characteristics of metal ions complexed to pyS SAMs

Figure 1 illustrates the spectral changes which occur in the normalized and background-subtracted SER spectra of pyS adsorbed on rough gold after complexation of Pd^{2+} ions from neutral solution. The supporting information shows the as-recorded spectra as well as their difference spectrum.

The peaks have been labelled with Gardner and Wright's notation for monosubstituted benzenes[52,53]. Most visible peaks are totally symmetric with respect to the pyridine C_{2v} axis, except for two out-of-plane CH deformation modes at ca. 500 and 810 cm^{-1} (modes $\mathcal{M}17$ and $\mathcal{M}19$). The highest frequency peaks are the C=C stretches (mode $\mathcal{M}4$) around 1600 cm^{-1}. They occur for neutral and protonated pyridine rings at 1574.4 and 1606.6 cm^{-1}, while the difference spectrum shows that complexation of Pd^{2+} ions generates a new C=C stretch at 1591.8 cm^{-1}. The ring breathing vibration (mode $\mathcal{M}9$) of a pyS SAM is a rather broad band around 1000 cm^{-1}, which contains contributions from bare, protonated and hydrogen-bonded species, as recently shown by us[50]. The complexed SAM possesses a ring breathing vibration at 1037.7 cm^{-1}, which is much narrower, indicating a single species. The trigonal ring deformation (mode $\mathcal{M}6$) shows a small frequency upshift from 1092.6 cm^{-1} to 1095.1 cm^{-1}.

In crystalline 4-mercaptopyridine, this mode is found at 1105 cm^{-1} and the frequency downshift (and concomitant intensity increase) is one of the characteristic features of a thiolate. The increase in frequency after complexation could indicate that the pyS-Au bond is slightly weakened. A large

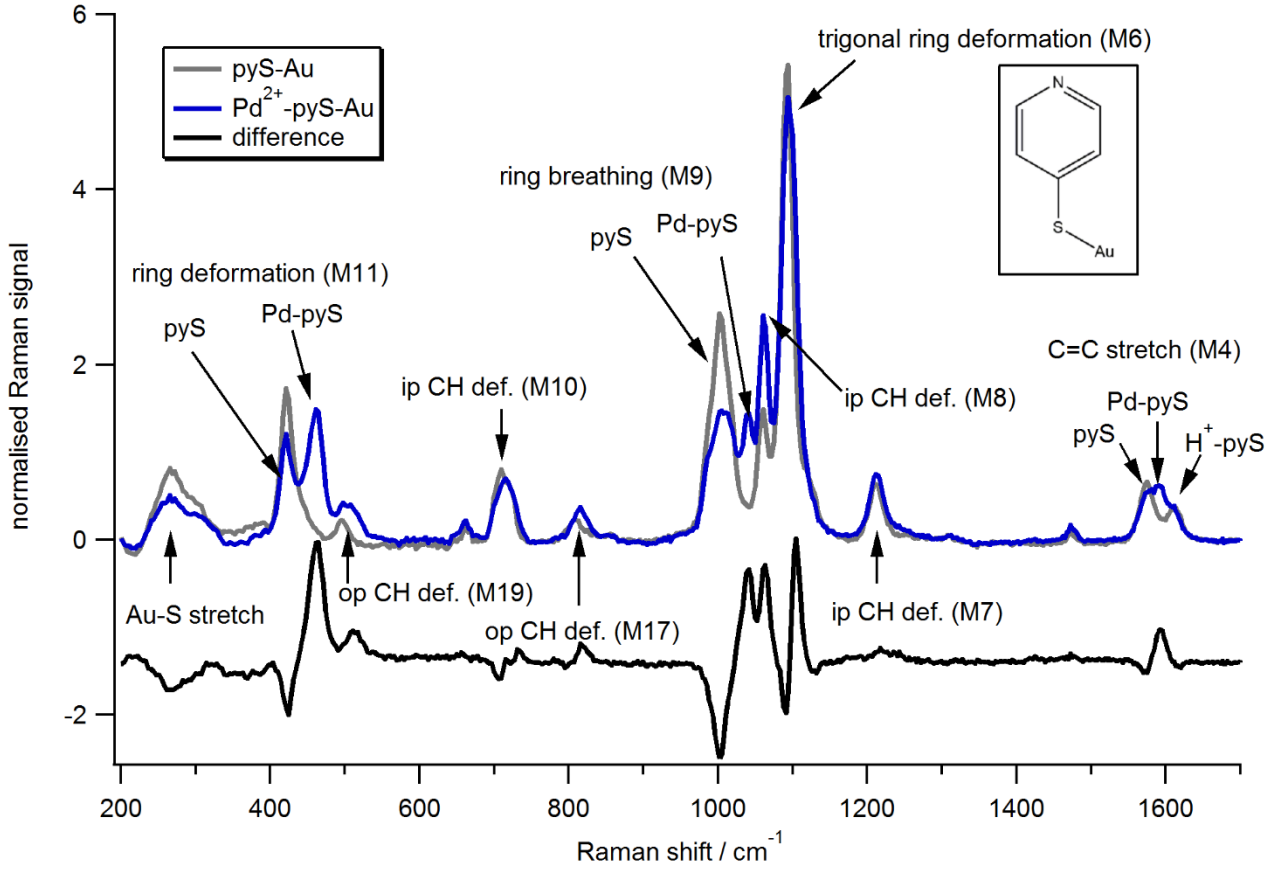

Figure 1. Complexation of Pd^{2+} ions from $PdSO_4$/0.1M H_2SO_4 /0.1 M NaOH (i.e. neutral solution) to pyS SAMs. Grey: SER spectrum of pyS adsorbed on roughened gold. Blue: same sample after complexation of Pd^{2+}. Black: Difference spectrum.

intensity change (with minor frequency shift) is seen for the in-plane CH deformation mode $\mathcal{M}8$.

The frequency changes in the C=C stretching and ring breathing modes can be explained by the hyperconjugation model for pyS. Some of the nitrogen lone-pair density resides in antibonding σ orbitals of the C_2-C_3 and C_5-C_6 bonds.

Complexation between Pd^{2+} and the nitrogen lone pair removes some of this electron density and strengthens the aromatic ring, which increases the ring breathing frequency. The Pd ion captures significantly more electron density than a proton, because the frequency shifts almost ten-fold in comparison. Strengthening of the C_2-C_3 and C_5-C_6 bonds also increases the C=C stretch frequency, but the frequency increase is less than upon protonation because the metal ion has a higher mass. Strengthening of the aromatic ring probably also explains the frequency upshift of mode $\mathcal{M}11$, a ring deformation coupled to a C-S stretch, from 420 cm^{-1} to 462.4 cm^{-1}.

To confirm the mode assignment, we carried out DFT calculations and experimental and calculated frequencies of the key totally symmetric modes are compared in Table 1. As seen for protonation[50], DFT underestimates the ring breathing shift but otherwise confirms the frequency shifts seen in the spectra.

We have obtained clearer spectral changes from adsorption on pinhole SHINs, as shown in the SI (Figure S2). There appears to be an ideal pinhole size which permits almost complete complexation of the pyS layer, however, control of the pinhole size is extremely difficult and is forming part of a separate investigation.

4-mercaptopyridine has been popular as a surface-enhanced Raman reporter for metal ions. While several experimental strategies monitor pyS SERS intensity, changed by metal-ion induced aggregation[54], desorption of pyS caused by Hg complex formation[55] or alloy formation[56], a few studies looked for vibrational signatures of metal ions coordinated to the nitrogen lone pair. The new ring breathing mode which occurs on metal ion complexation was first reported by Baldwin *et al.* for complexation of Cu^{2+} ions to 4-mercaptopyridine adsorbed on Ag colloid and was assigned by comparison to pyridine-copper metal complexes[24]. The pyS-Ag SAM has a ring breathing frequency of 1013 cm^{-1}, which shifts to 1034 cm^{-1} for the Cu^{2+}-pyS-Ag complex.

More recently, Jin *et al.* reported new modes at 1027 cm^{-1} and at 1584 cm^{-1} for a Zn^{2+}-pyS-Au complex[25]. The new bands are found at similar frequencies reported for metal pyridine tetracyanonickel complexes[57] and our assignment above shows that these are ring breathing and stretching modes, respectively. Guerrini *et al.* on the contrary reported no spectral changes of pyS-AuNP by Zn^{2+} and other metal ions, with the

exception of Hg^{2+} and CH_3Hg^+, but their SER spectra are indicative of a 1,4'-bipyridine thiolate species, created through a coupling reaction between adsorbed pyS and pyS in solution[58].

Table 1 Experimental and calculated frequencies for the Pd^{2+}-pyS-Au complex and pyS-Au. Frequencies were uniformly scaled by 0.982 (average from our previous calculation), apart from the C=C stretch which was scaled by 0.982*0.99).

Mode	Pd^{2+}-pyS-Au theory	Pd^{2+}-pyS-Au exp	pyS-Au exp	H^+-pyS-Au theory	pyS-Au theory
C=C stretch ($\mathcal{M}$4)	1597.4	1591.8	1574.4 1606.6	1632.4	1580.4
Trigonal ring def. ($\mathcal{M}$6)	1111.1	ca. 1100	1092.6	1098.7	1093.6
Ip CH def. ($\mathcal{M}$8)	1068.4	1062.3	1063.5	1064.7	1069.9
Ring breath ($\mathcal{M}$9)	1024.8	1037.7	~1000	996.3	1000.3
Op CH def. ($\mathcal{M}$17)	806.2	816.8	810.0	816.6	821.6
Op CH def. ($\mathcal{M}$19)	477.4	510.0	495.9	474.3	514.9
Ring def. ($\mathcal{M}$11)	462.4	462.4	420.1	400.3	408.5

We have detected this species on occasion and it can be distinguished by characteristic bands at 1040 and 1280 cm^{-1} (experimental and theoretical spectra are shown in Figure S3). While 1,4'-bipyridine thiolate also possesses a nitrogen lone pair oriented towards the solution, which could complex Pd^{2+} ions, the positive charge on the molecule probably prevents or slows down complexation (see below).

The strongest mode, the trigonal ring deformation $\mathcal{M}$6, shifts to higher frequencies when Pd or other metal ions are complexed to pyS-Au and its frequency is correlated to the height of the new $\mathcal{M}$11 mode, as shown in Figure 2. This correlation indicates that $\mathcal{M}$6 must consist of two overlapping peaks, the lower frequency one corresponding to bare pyS-Au, the higher frequency one to M^{n+}-pyS-Au. As discussed above, the frequency upshift indicates a weakening of the Au-pyS bond. The more metal ions complex to the layer, the higher the intensity of the high frequency shoulder and therefore the higher the frequency of the overall unresolved peak. The exception to the general trend is complexation of Ag, which has a high trigonal ring deformation frequency but no onew peaks. The increase in frequency indicates a significant weakening of the pyS-substrate bond (free mercaptopyridine has a trigonal ring deformation of 1105 cm^{-1}). The adsorbate could bind to Ag atoms spontaneously reduced on the Au surface, but the driving force for this is unclear if the pyS-Ag bond is indeed weaker than the pyS-Au bond.

To summarize, if pyS is to be used as a Raman sensor for metal ions, the three best reporter modes are the low frequency ring deformation mode, the new ring breathing mode and the C=C stretching mode. We now show how we can employ the new vibrational modes to monitor the fraction of pyS-Au which is complexed to a metal ion.

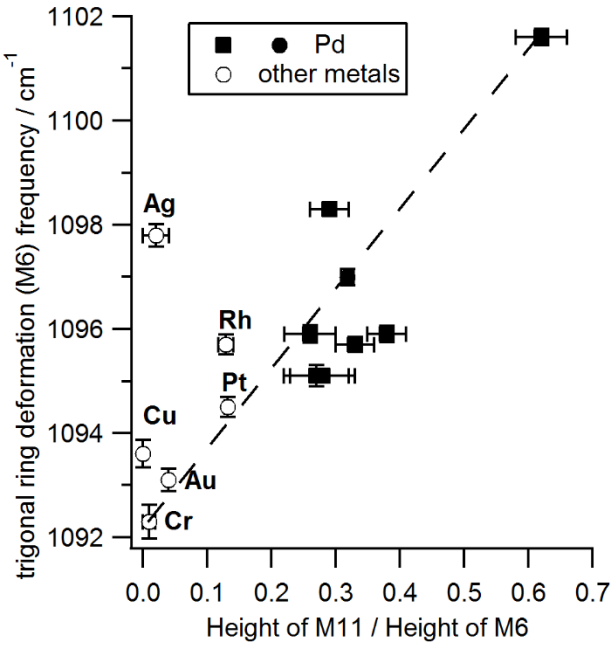

Figure 2 The trigonal ring deformation $\mathcal{M}$6 shows an upshift in frequency when a successful junction is formed, as indicated by the height of the new $\mathcal{M}$11 mode (line drawn to guide the eye). Exception is Ag, where the frequency is high, but no new $\mathcal{M}$11 peak is present. Spectra shown in Figures S-4 (○,●), S-5 (■).

Pd ion complexation – fast and slow exchange

The C=C stretching region has been used previously to monitor the degree of protonation of pyS-Au and thereby the local pH[59-62] and we show here that it can also be used to monitor complexation kinetics. The substrate this time was formed from pinhole SHINs dried on a silicon wafer. This substrate can be made quickly, and is well suited to optimize complexation conditions, even though it cannot be easily used for electrochemical reduction.

Figure 3 shows the complexation kinetics of Pd^{2+} from 0.1 M $PdSO_4$ solution. We fitted the C=C stretching region with three Gaussians with equal widths and normalized their peak heights by the integral of the trigonal ring deformation at each time point to account for any sample movement leading to small coverage changes in the detected spot.

The spectra show a fast change within the timescale of the first spectrum (30 s acquisition time) and then a much slower change with a half-time of 195 s. The fast change is partly due to the low pH of the metal salt solution, which increases the H^+-pyS-Au peak. There is also a factor 3 decrease of the

pyS-Au peak and the Pd^{2+}-pyS-Au peak already reaches half the height of its saturation value. The much bigger change in deprotonated peak height compared to protonated peak height is presumably caused by a fast complexation of deprotonated pyS-Au to Pd^{2+} ions in solution. This is followed by a much slower exchange with protonated H^+-pyS-Au, because the protonated peak is seen to decrease on the same time scale as the number of metal ion complexes increases. The peak height of the deprotonated species changes by less than 20%, indicating that a certain fraction of the layer is inaccessible to complexation, presumably due to steric hindrance.

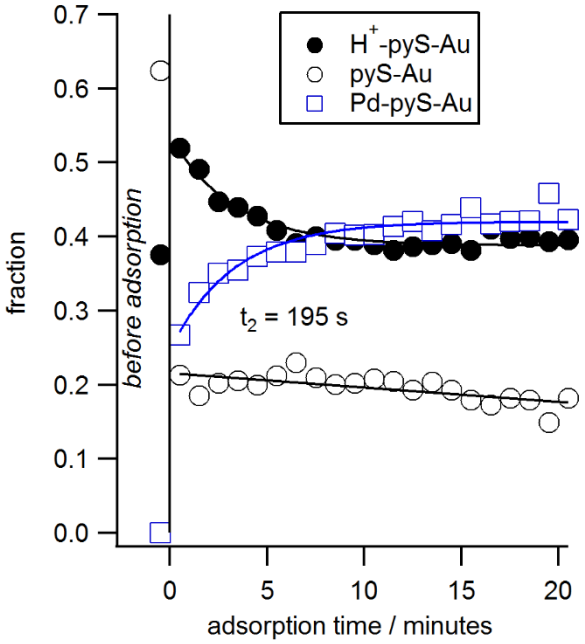

Figure 3. Complexation kinetics. The C=C stretching region was fitted with three Gaussian peaks with equal widths and normalized by the integral of the trigonal ring deformation mode.

These data address one of the fundamental questions posed during development of this method[63] – how do the Pd^{II} and pyridine species interact? An electrostatic interaction was ruled out due to the charged nature of the SAM at acidic pH, instead complexation with formation of a neutral sulfato-amino $Pd(SO_4)(Py)_2$ complex was proposed, where Pd substitutes the hydrogen on the pyridine. The data in Figure 2 suggest however that complexation competes with protonation of neutral pyS-Au when the sample is first transferred into the acidic metal salt solution. Only in a second step are protons replaced by Pd ions, which is a much slower process due to the charge repulsion. Our observed time-scale agrees well with a reported time of 20 min required to saturate all available pyridine moieties[40]. Detailed kinetics have so far only been measured for a longer py-terminated SAM[44]. In all reported cases, the measured reduction charge indicates that a pyridine-terminated SAM is nearly fully coordinated to Pd ions. This should be contrasted to a 40% Pd coverage in our Raman spectra (assuming the C=C Raman polarizability is the same for all three species), which is typical for many samples we prepared on both rough gold and SHINs. This could indicate that some of our pyS are not sterically accessible on the rough surfaces or that two neighbouring pyS at the right distance are required to form the sulfato-amino complex. We consider the latter explanation less likely, because we typically achieve pyS coverages of around 0.27 ML (measured by reductive desorption in 0.1 M NaOH from a polycrystalline gold electrode), i.e the average layer density is close to the published value for Au(111)[48].

Even though this lower coverage of Pd^{2+} ions is an obvious disadvantage to using rough substrates, the relative ease with which one can establish a time-constant for complexation and estimate the fraction of the SAM coordinated to metal ions allows one to rapidly optimize process parameters before embarking on longer studies on single-crystalline surfaces.

Reduction of metal ions on non-ideal surfaces

For electrodeposition of metals, Kolb *et al.* developed a two-step method to reduce the chances of metal ion reduction at defect sites in the SAM[34,35,48,63]. The electrode is first immersed in metal salt solution for a given time to allow to form a complex with the adsorbate, it is then rinsed and transferred to 0.1 M H_2SO_4 in an electrochemical cell at positive potential to prevent spontaneous reduction of Pd[48]. A scan in negative direction then reduces only the ions complexed to the SAM. This method has been very successful for pyS adsorbed at single crystalline gold. Direct reduction in 1 mM $PdSO_4$ solution was recently shown to be successful for a pyridine-terminated SAM, 3-(4-pyridine-4-yl phenyl)propane-1-thiol, where the tight packing of the phenylalkane spacer appears to prevent direct Pd deposition on the gold substrate[40].

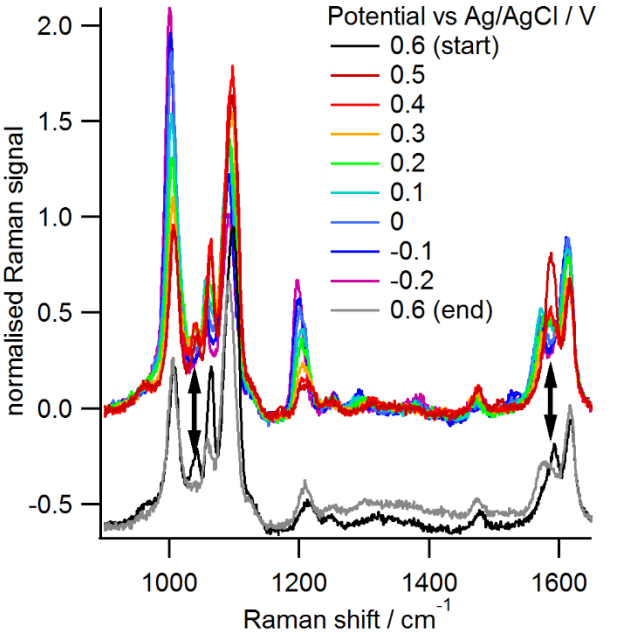

Figure 4. Disappearance of the Pd ion peaks (marked by vertical arrows) as the sample potential is step-wise decreased from 0.6 to -0.2 V and then increased back to + 0.6 V. The initial and final spectra at + 0.6 V are offset for clarity.

A disadvantage of SAMs on rough surfaces is the presence of many defect sites which allow reduction of metal ions at the gold substrate, leading to mushroom growth[1]. We found that the two-step process quite often led to either a reduction in the characteristic Pd-pyS-Au peaks or their complete disappearance. Figure 4 shows Raman spectra acquired during a step-wise reduction in electrode potential in 0.1 M H_2SO_4. Pd reduction on top of the SAM should occur around 0.0 V vs Ag/AgCl. At the start of the scan at + 0.6 V, the peaks from complexed Pd ions at 1040 and 1587 cm^{-1} are clearly visible. They start decreasing in height from about 0.2 V and have nearly disappeared by -0.2 V. Increasing the potential back to + 0.6 V shows that most of the complexed Pd has been lost, either due to direct reduction on the substrate or due to dissolvation of Pd ions back into H_2SO_4 solution[64]. Since this

phenomenon has not been reported for single-crystalline substrates, we speculate that this is a consequence of defects in the SAM. Figure 4 also shows an intensity increase of ring breathing vibration, CH in-plane bend and protonated C=C stretch with decreasing potential, but this is not related to the presence of Pd ions or atoms, as the same increase is observed on a pure pyS-Au layer.

In attempts to overcome the disappearance of metal-related peaks during reduction, we discovered that a reduction of the Pd ions in metal salt solution, similar to the literature observation for longer pyridine-terminated SAMs[40], tends to maintain or even increase the height of Pd-related peaks. Figure 5A shows an example of successful Pd-pyS-Au junction formation by direct reduction in $PdSO_4$ solution, while Figure 5C shows an unsuccessful metallization using the two-step method. Deconvolution of the C=C region for the spectra in Figure 4 shows that the Pd peak increases from 42% to 53% on reduction in $PdSO_4$ solution, while in H_2SO_4 the fraction decreases from 46% to 37%.

This was also confirmed by the cyclic voltammograms in Figure 5 B,D. The characteristic peak of Pd^{2+} converting to Pd^0 appears at around -570 mV vs $Hg/HgSO_4$, corresponding to -150 mV vs SCE, which is lower than Kolb's value of -50 mV vs SCE on Au(111)[63]. The difference can probably be explained by the wide range of crystal facets present on roughened gold and the known structure dependence of oxidation and reduction potentials[65].

It is worth noting from a comparison of complexed Pd^{2+} ion and Pd metal spectra that there is hardly any frequency shift, that is we can establish the vibrational signature of a metal-molecule-metal junction from metal ion complexation alone.

Mushroom growth and metal creep

Since mushroom growth is clearly a problem for metallising SAMs on rough surfaces, we investigated to which degree this influences the spectrum. In Figure 6A, we compare the bare pyS-Au layer at +0.6 V versus the partially metallised layer, which lost most Pd either to solution or to direct reduction on the gold substrate (end point of Figure 3). While some small changes in peak heights have occurred, the most noticeable effect is that the layer looks significantly more protonated, as seen by the disappearance of the low frequency shoulder of the ring breathing vibration (assigned to bare pyS-Au[50]) and the increase in height and frequency of the protonated C=C vibration. This means that mushroom growth does not appear to cause any clear spectral shifts. We also checked for the effect of metal creep in between adsorbate and gold substrate. Figure 6B compares pyS spectra adsorbed on gold and on a thick Pd layer electrochemically deposited on gold. While the Pd/Au layer is partially oxidised, the pyS peaks are all found at the same frequencies as on gold itself.

We conclude from these spectra that SERS is expected to be relatively insensitive to any kind of defects occurring during reduction of the complexed metal ion layer.

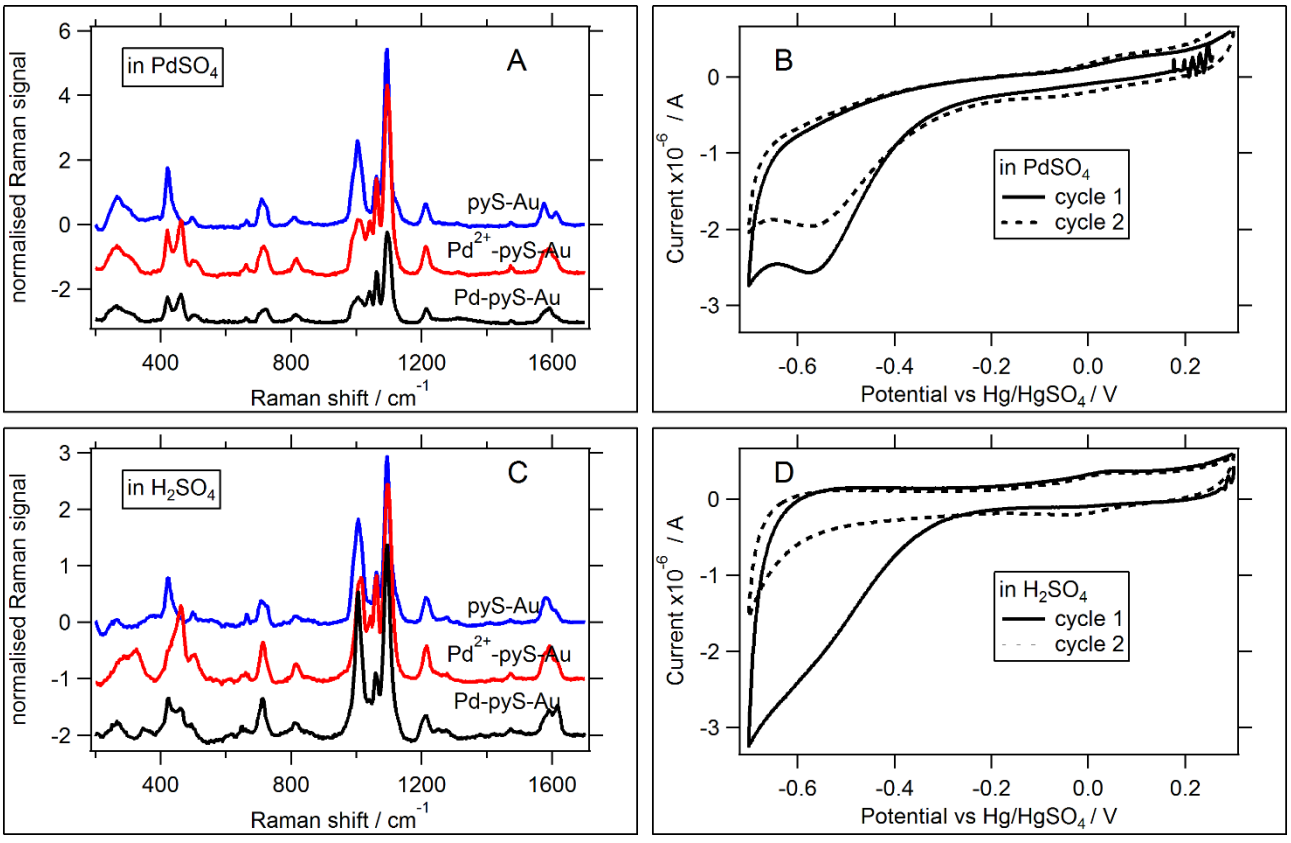

Figure 5. SER spectra of pyS SAMs on rough gold, complexed in metal ion solution and then reduced in the same solution (A) or in a two-step method in sulfuric acid (C). Reduction in metal ion solution forms a successful junction as can be seen in its CV trace (B) with a Pd reduction peak at -0.57 V, while reduction in H_2SO_4 (trace D) mostly fails to reduce Pd on top of the layer (no clear peak in CV)

CONCLUSIONS

In conclusion, it is not necessary to use single-crystalline surfaces for spectroscopy of metal-molecule-metal junctions. Due to the insensitivity of SERS to defects, we can use SERS on roughened gold and gold nanoparticles to establish the key vibrational signatures of MMM junctions and obtain coarse information on complexation kinetics and electrochemical re-

duction. This information can help to quickly optimize sample preparation before embarking on more detailed single crystal studies.

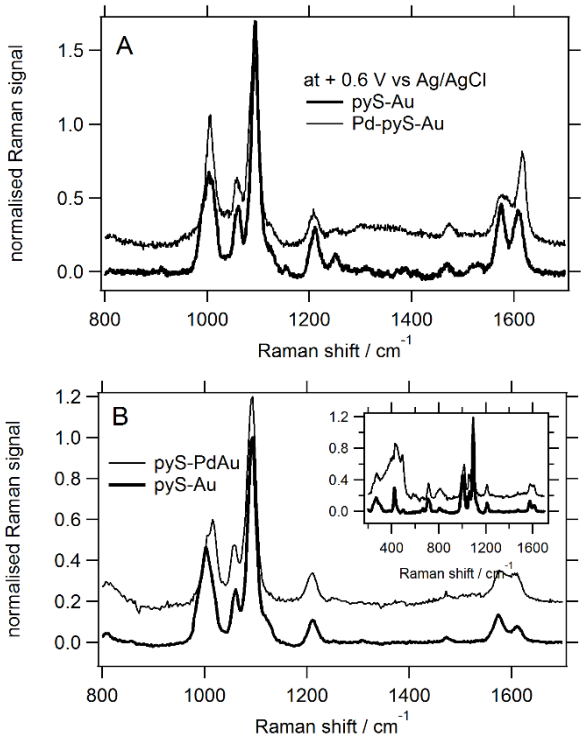

Figure 6. A. Comparison of pyS-Au at + 0.6 V vs Ag/AgCl and a pyS-Au SAM which is to a small degree metallised and the rest probably on the substrate. B. Comparison of pyS-Au and pyS-Pd/Au spectra.

ASSOCIATED CONTENT

Supporting Information

The Supporting Information is available free of charge on the ACS Publications website.

Supporting information contains raw data for Figure 1, SER spectra of Pd complexation to 4-mercaptopyridine in pinholes on SHINs and experimental and theoretical Raman spectra of 1-4'-bipyridine thiolate. The supporting information is provided as PDF file.

AUTHOR INFORMATION

Corresponding Author

*Heike Arnolds, Heike.Arnolds@liverpool.ac.uk

Present Addresses

† Nungnit Wattanavichean:
Department of Applied Chemistry
National Chiao Tung University
1001 Daxue Road, Hsinchu, Taiwan, 300

§ Matthew Gilby:
Eli Lilly and Company
Fleming Road
Speke
Liverpool, L24 9LN, UK

ACKNOWLEDGMENT

N. W. gratefully acknowledges Mahidol University, Thailand, and University of Liverpool, UK, for receipt of a Mahidol-Liverpool Stang Mongkolsuk PhD Scholarship. Part of this work was supported by the Leverhulme Trust (RPG-2012-632).

REFERENCES

(1) Vilan, A.; Aswal, D.; Cahen, D. Large-Area, Ensemble Molecular Electronics: Motivation and Challenges *Chem. Rev.* **2017**, *117*, 4248-4286.

(2) Nichols, R. J.; Higgins, S. J. Single-Molecule Electronics: Chemical and Analytical Perspectives *Annu. Rev. Anal. Chem.* **2015**, *8*, 389-417.

(3) Xiang, D.; Wang, X. L.; Jia, C. C.; Lee, T.; Guo, X. F. Molecular-Scale Electronics: From Concept to Function *Chem. Rev.* **2016**, *116*, 4318-4440.

(4) Aradhya, S. V.; Venkataraman, L. Single-molecule junctions beyond electronic transport *Nat. Nanotechnol.* **2013**, *8*, 399.

(5) Liu, Z.; Ding, S. Y.; Chen, Z. B.; Wang, X.; Tian, J. H.; Anema, J. R.; Zhou, X. S.; Wu, D. Y.; Mao, B. W.; Xu, X.; Ren, B.; Tian, Z. Q. Revealing the molecular structure of single-molecule junctions in different conductance states by fishing-mode tip-enhanced Raman spectroscopy *Nat. Commun.* **2011**, *2*, 305.

(6) Galperin, M.; Ratner, M. A.; Nitzan, A. Molecular transport junctions: vibrational effects *J. Phys.: Condens. Matter* **2007**, *19*, 103201.

(7) Tsutsui, M.; Taniguchi, M.; Shoji, K.; Yokota, K.; Kawai, T. Identifying molecular signatures in metal-molecule-metal junctions *Nanoscale* **2009**, *1*, 164-170.

(8) Jun, Y.; Zhu, X. Y. FTIR Spectroscopy of Buried Interfaces in Molecular Junctions *J. Am. Chem. Soc.* **2004**, *126*, 13224-13225.

(9) Scott, A.; Hacker, C. A.; Janes, D. B. In situ Structural Characterization of Metal−Molecule−Silicon Junctions Using Backside Infrared Spectroscopy *J. Phys. Chem. C* **2008**, *112*, 14021-14026.

(10) Mahmoud, A. M.; Bergren, A. J.; McCreery, R. L. Derivatization of Optically Transparent Materials with Diazonium Reagents for Spectroscopy of Buried Interfaces *Anal. Chem.* **2009**, *81*, 6972-6980.

(11) Nowak, A. M.; McCreery, R. L. In Situ Raman Spectroscopy of Bias-Induced Structural Changes in Nitroazobenzene Molecular Electronic Junctions *J. Am. Chem. Soc.* **2004**, *126*, 16621-16631.

(12) Asanuma, H.; Noguchi, H.; Huang, Y.; Uosaki, K.; Yu, H.-Z. Probing the Molecular Conformation of Self-Assembled Monolayers at Metal/Semiconductor Interfaces by Vibrational Sum Frequency Generation Spectroscopy *J. Phys. Chem. C* **2009**, *113*, 21139-21146.

(13) Cui, L.; Liu, B.; Vonlanthen, D.; Mayor, M.; Fu, Y.; Li, J. F.; Wandlowski, T. In situ gap-mode Raman spectroscopy on single-crystal Au(100) electrodes: tuning the torsion angle of 4,4'-biphenyldithiols by an electrochemical gate field *J. Am. Chem. Soc.* **2011**, *133*, 7332-7335.

(14) Matsuhita, R.; Horikawa, M.; Naitoh, Y.; Nakamura, H.; Kiguchi, M. Conductance and SERS Measurement of Benzenedithiol Molecules Bridging Between Au Electrodes *J. Phys. Chem. C* **2013**, *117*, 1791-1795.

(15) Ikeda, K.; Fujimoto, N.; Uosaki, K. Nanoscale Optical and Mechanical Manipulation of Molecular Alignment in Metal–Molecule–Metal Structures *J. Phys. Chem. C* **2014**, *118*, 21550-21557.

(16) Dasari, R.; Zamborini, F. P. Surface Enhanced Raman Spectroscopy at Electrochemically Fabricated Silver Nanowire Junctions *Anal. Chem.* **2016**, *88*, 675-681.

(17) Li, Y.; Zolotavin, P.; Doak, P.; Kronik, L.; Neaton, J. B.; Natelson, D. Interplay of Bias-Driven Charging and the Vibrational Stark Effect in Molecular Junctions *Nano Lett.* **2016**, *16*, 1104-1109.

(18) Marqués-González, S.; Matsushita, R.; Kiguchi, M. Surface enhanced Raman scattering of molecules in metallic nanogaps *J. Opt.* **2015**, *17*, 114001.

(19) Zheng, J.; Liu, J.; Zhuo, Y.; Li, R.; Jin, X.; Yang, Y.; Chen, Z. B.; Shi, J.; Xiao, Z.; Hong, W.; Tian, Z. Q. Electrical and SERS detection of disulfide-mediated dimerization in single-molecule benzene-1,4-dithiol junctions *Chem. Sci.* **2018**, *9*, 5033-5038.

(20) Khlebtsov, B.; Khanadeev, V.; Khlebtsov, N. Surface-enhanced Raman scattering inside Au@Ag core/shell nanorods *Nano Res.* **2016**, *9*, 2303-2318.

(21) Huang, Y. F.; Yin, N. N.; Wang, X.; Wu, D. Y.; Ren, B.; Tian, Z. Q. Vibrational signature of double-end-linked molecules at Au nanojunctions probed by surface-enhanced Raman spectroscopy *Chem. Eur. J.* **2010**, *16*, 1449-1453.

(22) Zheng, X.-S.; Hu, P.; Zhong, J.-H.; Zong, C.; Wang, X.; Liu, B.-J.; Ren, B. Laser Power Dependent Surface-Enhanced Raman Spectroscopic Study of 4-Mercaptopyridine on Uniform Gold Nanoparticle-Assembled Substrates *J. Phys. Chem. C* **2014**, *118*, 3750-3757.

(23) Singh, P.; Deckert, V. Local protonation control using plasmonic activation *Chem. Commun.* **2014**, *50*, 11204-11207.

(24) Baldwin, J.; Schühler, N.; Butler, I. S.; Andrews, M. P. Integrated Optics Evanescent Wave Surface Enhanced Raman Scattering (IO-EWSERS) of Mercaptopyridines on a Planar Optical Chemical Bench: Binding of Hydrogen and Copper Ion *Langmuir* **1996**, *12*, 6389-6398.

(25) Jin, L.; She, G.; Mu, L.; Shi, W. Highly uniform indicator-mediated SERS sensor platform for the detection of Zn2+ *RSC Adv.* **2016**, *6*, 16555-16560.

(26) Smith, E. L.; Alves, C. A.; Anderegg, J. W.; Porter, M. D.; Siperko, L. M. Deposition of metal overlayers at end-group-functionalized thiolate monolayers adsorbed at gold. 1. Surface and interfacial chemical characterization of deposited copper overlayers at carboxylic acid-terminated structures *Langmuir* **1992**, *8*, 2707-2714.

(27) Herdt, G. C.; Czanderna, A. W. Metal overlayers on organic functional groups of self-assembled monolayers: VIII. X-ray photoelectron spectroscopy of the Ni/COOH interface *J. Vac. Sci. Technol., A* **1999**, *17*, 3415-3418.

(28) Jung, D. R.; Czanderna, A. W. Chemical and physical interactions at metal/self-assembled organic monolayer interfaces *Crit. Rev. Solid State Mater. Sci.* **1994**, *19*, 1-54.

(29) Nishizawa, M.; Sunagawa, T.; Yoneyama, H. Underpotential Deposition of Copper on Gold Electrodes through Self-Assembled Monolayers of Propanethiol *Langmuir* **1997**, *13*, 5215-5217.

(30) Baunach, T.; Kolb, D. The electrochemical characterisation of benzyl mercaptan-modified Au(111): Structure and copper deposition *Anal. Bioanal. Chem.* **2002**, *373*, 743-748.

(31) Hagenström, H.; Schneeweiss, M. A.; Kolb, D. M. Copper underpotential deposition on ethanethiol-modified Au(111) electrodes: kinetic effects *Electrochim. Acta* **1999**, *45*, 1141-1145.

(32) Gilbert, S. E.; Cavalleri, O.; Kern, K. Electrodeposition of Cu Nanoparticles on Decanethiol-Covered Au(111) Surfaces: An in Situ STM Investigation *J. Phys. Chem.* **1996**, *100*, 12123-12130.

(33) Oyamatsu, D.; Nishizawa, M.; Kuwabata, S.; Yoneyama, H. Underpotential Deposition of Silver onto Gold Substrates Covered with Self-Assembled Monolayers of Alkanethiols To Induce Intervention of the Silver between the Monolayer and the Gold Substrate *Langmuir* **1998**, *14*, 3298-3302.

(34) Manolova, M.; Ivanova, V.; Kolb, D. M.; Boyen, H. G.; Ziemann, P.; Buttner, M.; Romanyuk, A.; Oelhafen, P. Metal deposition onto thiol-covered gold: Platinum on a 4-mercaptopyridine SAM *Surf. Sci.* **2005**, *590*, 146-153.

(35) Manolova, M.; Kayser, M.; Kolb, D. M.; Boyen, H. G.; Ziemann, P.; Mayer, D.; Wirth, A. Rhodium deposition onto a 4-mercaptopyridine SAM on Au(111) *Electrochim. Acta* **2007**, *52*, 2740-2745.

(36) Ivanova, V.; Manolova, M.; Kolb, D. Palladium and Platinum Deposition onto 4-mercaptopyridine SAMs *Solid State Phenom.* **2007**, *121-123*, 363-368.

(37) Chesneau, F.; Zharnikov, M. Palladium Chloride as Seeding and Surfactant Layer to Mediate the Formation of Top Metal Films on Self-Assembled Monolayers *J. Phys. Chem. C* **2014**, *118*, 12980-12988.

(38) Langerock, S.; Ménard, H.; Rowntree, P.; Heerman, L. Electrocrystallization of Rhodium Clusters on Thiolate-Covered Polycrystalline Gold *Langmuir* **2005**, *21*, 5124-5133.

(39) Keith, J. A.; Jacob, T. Atomic-Level Elucidation of the Initial Stages of Self-Assembled Monolayer Metallization and Nanoparticle Formation *Chem. Eur. J.* **2010**, *16*, 12381-12386.

(40) Silien, C.; Lahaye, D.; Caffio, M.; Schaub, R.; Champness, N. R.; Buck, M. Electrodeposition of Palladium onto a Pyridine-Terminated Self-Assembled Monolayer *Langmuir* **2011**, *27*, 2567-2574.

(41) Muglali, M. I.; Bashir, A.; Birkner, A.; Rohwerder, M. Hydrogen as an optimum reducing agent for metallization of self-assembled monolayers *J. Mater. Chem.* **2012**, *22*, 14337-14340.

(42) Eberle, F.; Saitner, M.; Boyen, H.-G.; Kucera, J.; Gross, A.; Romanyuk, A.; Oelhafen, P.; D'Olieslaeger, M.; Manolova, M.; Kolb, D. M. A Molecular Double Decker: Extending the Limits of Current Metal-Molecule Hybrid Structures *Angew. Chem. Int. Ed.* **2010**, *49*, 341-345.

(43) Eberle, F.; Kayser, M.; Kolb, D. M.; Saitner, M.; Boyen, H.-G.; D'Olieslaeger, M.; Mayer, D.; Wirth, A. Metallization of Organic Surfaces: Pd on Thiazole *Langmuir* **2010**, *26*, 4738-4742.

(44) Muglali, M. I.; Liu, J. X.; Bashir, A.; Borissov, D.; Xu, M. C.; Wang, Y. M.; Woll, C.; Rohwerder, M. On the complexation kinetics for metallization of organic layers: palladium onto a pyridine-terminated araliphatic thiol film *Phys. Chem. Chem. Phys.* **2012**, *14*, 4703-4712.

(45) Li, J. F.; Tian, X. D.; Li, S. B.; Anema, J. R.; Yang, Z. L.; Ding, Y.; Wu, Y. F.; Zeng, Y. M.; Chen, Q. Z.; Ren, B.; Wang, Z. L.; Tian, Z. Q. Surface analysis using shell-isolated nanoparticle-enhanced Raman spectroscopy *Nat. Protoc.* **2012**, *8*, 52.

(46) Yang, D. F.; Wilde, C. P.; Morin, M. Electrochemical Desorption and Adsorption of Nonyl Mercaptan at Gold Single Crystal Electrode Surfaces *Langmuir* **1996**, *12*, 6570-6577.

(47) Zhou, W. P.; Baunach, T.; Ivanova, V.; Kolb, D. M. Structure and electrochemistry of 4,4 '-dithiodipyridine self-assembled monolayers in comparison with 4-mercaptopyridine self-assembled monolayers on Au(111) *Langmuir* **2004**, *20*, 4590-4595.

(48) Ivanova, V.; Baunach, T.; Kolb, D. M. Metal deposition onto a thiol-covered gold surface: A new approach *Electrochim. Acta* **2005**, *50*, 4283-4288.

(49) Manolova, M.; Boyen, H.-G.; Kucera, J.; Gross, A.; Romanyuk, A.; Oelhafen, P.; Ivanova, V.; Kolb, D. M. Chemical Interactions at Metal/Molecule Interfaces in Molecular Junctions-A Pathway Towards Molecular Recognition *Adv. Mater.* **2009**, *21*, 320-324.

(50) Wattanavichean, N.; Casey, E.; Nichols, R. J.; Arnolds, H. Discrimination between hydrogen bonding and protonation in the spectra of a surface-enhanced Raman sensor *Phys. Chem. Chem. Phys.* **2018**, *20*, 866-871.

(51) Wei, H.; Leng, W.; Song, J.; Willner, M. R.; Marr, L. C.; Zhou, W.; Vikesland, P. J. Improved Quantitative SERS Enabled by Surface Plasmon Enhanced Elastic Light Scattering *Anal. Chem.* **2018**, *90*, 3227-3237.

(52) Birke, R. L.; Lombardi, J. R. Simulation of SERS by a DFT study: a comparison of static and near-resonance Raman for 4-mercaptopyridine on small Ag clusters *J. Opt.* **2015**, *17*, 114004.

(53) Gardner, A. M.; Wright, T. G. Consistent assignment of the vibrations of monosubstituted benzenes *J. Chem. Phys.* **2011**, *135*, 114305.

(54) Li, J.; Chen, L.; Lou, T.; Wang, Y. Highly Sensitive SERS Detection of As3+ Ions in Aqueous Media using Glutathione Functionalized Silver Nanoparticles *ACS Appl. Mater. Interfaces* **2011**, *3*, 3936-3941.

(55) Li, K.; Liang, A.; Jiang, C.; Li, F.; Liu, Q.; Jiang, Z. A stable and reproducible nanosilver-aggregation-4-mercaptopyridine surface-enhanced Raman scattering probe for rapid determination of trace Hg2+ *Talanta* **2012**, *99*, 890-896.

(56) Chen, L.; Qi, N.; Wang, X.; Chen, L.; You, H.; Li, J. Ultrasensitive surface-enhanced Raman scattering nanosensor for mercury ion detection based on functionalized silver nanoparticles *RSC Adv.* **2014**, *4*, 15055-15060.

(57) Akyüz, S.; Dempster, A. B.; Morehouse, R. L.; Suzuki, S. An infrared and Raman spectroscopic study of some metal pyridine tetracyanonickelate complexes *J. Mol. Struct.* **1973**, *17*, 105-125.

(58) Gui, J. Y.; Lu, F.; Stern, D. A.; Hubbard, A. T. Surface chemistry of mercaptopyridines at Ag(111) electrodes studied by EELS, LEED, Auger spectroscopy and electrochemistry *J. Electroanal. Chem. Interfacial Electrochem.* **1990**, *292*, 245-262.

(59) Yu, H. Z.; Xia, N.; Liu, Z. F. SERS titration of 4-mercaptopyridine self-assembled monolayers at aqueous buffer/gold interfaces *Anal. Chem.* **1999**, *71*, 1354-1358.

(60) Chao, Y.; Zhou, Q.; Li, Y.; Yan, Y.; Wu, Y.; Zheng, J. Potential dependent surface-enhanced Raman scattering of 4-mercaptopyridine on electrochemically roughened silver electrodes *J. Phys. Chem. C* **2007**, *111*, 16990-16995.

(61) Jensen, R. A.; Sherin, J.; Emory, S. R. Single Nanoparticle Based Optical pH Probe *Appl. Spectrosc.* **2007**, *61*, 832-838.

(62) Zheng, X. S.; Hu, P.; Cui, Y.; Zong, C.; Feng, J. M.; Wang, X.; Ren, B. BSA-coated nanoparticles for improved SERS-based intracellular pH sensing *Anal. Chem.* **2014**, *86*, 12250-12257.

(63) Baunach, T.; Ivanova, V.; Kolb, D. M.; Boyen, H. G.; Ziemann, P.; Büttner, M.; Oelhafen, P. A New Approach to the Electrochemical Metallization of Organic Monolayers: Palladium Deposition onto a 4,4′-Dithiodipyridine Self-Assembled Monolayer *Adv. Mater.* **2004**, *16*, 2024-2028.

(64) Tang, J.; Petri, M.; Kibler, L. A.; Kolb, D. M. Pd deposition onto Au(111) electrodes from sulphuric acid solution *Electrochim. Acta* **2005**, *51*, 125-132.

(65) Diaz-Morales, O.; Calle-Vallejo, F.; de Munck, C.; Koper, M. T. M. Electrochemical water splitting by gold: evidence for an oxide decomposition mechanism *Chem. Sci.* **2013**, *4*, 2334.

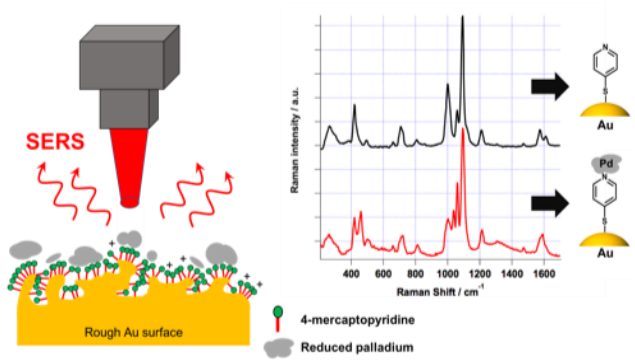
SERS
Rough Au surface
Raman intensity / a.u.
400
600
800
1000
1200
1400
1600
Raman Shift / cm-1
Au
Pd
Au
4-mercaptopyridine
Reduced palladium

For TOC ONLY